

Parameter estimation of photovoltaic modules using a hybrid flower pollination algorithm

Shuhui Xu, Yong Wang*

School of Mechanical Engineering, Shandong University, Jinan 250061, China

Key Laboratory of High-efficiency and Clean Mechanical Manufacture (Shandong University), Ministry of Education, Jinan 250061, China



ARTICLE INFO

Article history:

Received 15 December 2016

Received in revised form 19 March 2017

Accepted 11 April 2017

Available online 21 April 2017

Keywords:

Solar module

Flower pollination algorithm

Nelder-Mead simplex method

Generalized opposition-based learning

Parameter estimation

ABSTRACT

Building highly accurate model for solar cells and photovoltaic (PV) modules based on experimental data is vital for the simulation, evaluation, control, and optimization of PV systems. Powerful optimization algorithms are necessary to accomplish this task. In this study, a new optimization algorithm is proposed for efficiently and accurately estimating the parameters of solar cells and PV modules. The proposed algorithm is developed based on the flower pollination algorithm by incorporating it with the Nelder-Mead simplex method and the generalized opposition-based learning mechanism. The proposed algorithm has a simple structure thus is easy to implement. The experimental results tested on three different solar cell models including the single diode model, the double diode model, and a PV module clearly demonstrate the effectiveness of this algorithm. The comparisons with some other published methods demonstrate that the proposed algorithm is superior than most reported algorithms in terms of the accuracy of final solutions, convergence speed, and stability. Furthermore, the tests on three PV modules of different types (Multi-crystalline, Thin-film, and Mono-crystalline) suggest that the proposed algorithm can give superior results at different irradiance and temperature. The proposed algorithm can serve as a new alternative for parameter estimation of solar cells/PV modules.

© 2017 Elsevier Ltd. All rights reserved.

1. Introduction

Thanks to the serious environmental and social problems sparked by the widespread use and the growing shortage of fossil based fuels, such as greenhouse emissions, air pollution, threat of terrorist attack on the oil industry, tense political environments in oil producing countries, and so on, developing new alternative energy technologies has become an extremely urgent task for human beings [1,2]. Among various renewable energy sources such as wind, wave, nuclear, tidal, geothermal, biomass, and so on, solar energy is regarded as one of those with the most potential due to its wide availability and cleanliness. Solar photovoltaic systems which can directly convert solar energy into electricity have been applied worldwide after the sharp growth in recent years [3–5].

Solar photovoltaic systems contain different parts centered around a solar panel which typically has arrays of interconnected solar cells. Building highly accurate mathematical model to describe the non-linear current-voltage ($I-V$) relationship of the solar cells or the modules is an important fundamental task during

the design, simulation, evaluation, analysis, control, and optimization of solar photovoltaic systems [6–11]. Commonly, the behavior of solar cells is simulated using a lumped parameter equivalent circuit model under different operating conditions, and two main detail models, i.e. the single and double diode models, are widely used in practice [2,12]. The main parameters involved in these models include the generated photocurrent, saturation current, series resistance, shunt resistance, and ideality factor should be finally determined based on experimental data.

The current extraction techniques for PV parameters can be divided into analytical method, numerical extraction method, and combination of them. Analytical method mainly utilizes the information given in the manufacturer's data sheet such as open circuit voltage, short circuit current, maximum power voltage and maximum power current to model $I-V$ characteristics of any module. analytical method provides a simple and quick parameter calculation process but may lead to significant deviation between the simulated and actual performances [13]. Numerical extraction method utilizes individual point on the actual $I-V$ curve to obtain the model parameters. Essentially Numerical extraction method is curve fitting method and is suit for the PV cells/modules at any conditions, such as different irradiation and different temperature. In numerical extraction method, effective optimization tech-

* Corresponding author at: School of Mechanical Engineering, Shandong University, Jinan 250061, China.

E-mail address: meywang@126.com (Y. Wang).

nologies are very desirable and they decide the accuracy of the extracted parameters [14]. The current applied optimization technologies can be divided into two classes: traditional methods and meta-heuristic algorithms. Between them, meta-heuristic algorithms have drawn more attention due to the traditional methods have intrinsic limitations such as needing continuity, convexity, and differentiability conditions, heavy computations, highly sensitive to the initial values, and often lead to local optima [9,15]. Various meta-heuristic algorithms or their variants have been used to solve this problem, such as Genetic Algorithm [16,17], Particle Swarm Optimizer [18–20], Differential Evolution [21–23], Teaching Learning Based Optimization [9,12], Harmony Search algorithm [24], Artificial Bee Colony algorithm [25,26], Artificial Bee Swarm Optimization algorithm [15], Shuffled Frog Leaping algorithm [27], Biogeography-based Optimization algorithm [11], Moth-Flame Optimization algorithm [28], Bird Mating Optimizer [29,30], hybrid algorithm based on Electromagnetism-like Algorithm and Differential Evolution [13], and so on. Though there are so many different meta-heuristic algorithms have been applied to this problem and several among them perform excellently, looking for competitive algorithms based on different mechanisms is still an important issue in retailing research.

Flower pollination algorithm (FPA) is a novel meta-heuristic algorithm invented by Yang inspired by the flower pollination behavior of flowering plants [31,32]. This algorithm is very simple in form. There are only two different operators in the algorithm, and only a few parameters need to be set. Therefore, this algorithm is easy to implement and does not need tedious parameters tuning. Since FPA is proposed and especially in the past two years, it and its variants have been applied on many problems in different disciplines, such as controller design [33], structure design [34], machining process planning [35], economic load dispatch problems [36], neural network training [37], and so on.

The basic flower pollination algorithm has also been applied to the parameter estimation problems of PV systems [38]. In this study, we proposed a more effective hybrid algorithm for the parameter estimated problem of solar cells/PV modules by introducing the Nelder-Mead simplex method and the generalized opposition-based learning mechanism into the frame of the basic FPA. To demonstrate its usefulness and superiority, the proposed algorithm is firstly tested on three parameter estimation cases of solar cells/PV modules and compared with some other published methods, and then tested on three PV modules of different types (Multi-crystalline, Thin-film, and Mono-crystalline) at different irradiance and temperature. Both test results and comparison results demonstrate that the proposed algorithm has outstanding performance and superior practical utility.

The remainder of this paper is structured as follows. Section 2 describes the mathematical model of the parameter estimation problem of solar cells/PV modules. Section 3 detailedly introduces the proposed hybrid algorithm, followed by the experiments, discussions, and comparisons with other published technologies in Section 4. Finally, Section 5 concludes this paper.

2. Mathematics description of the problem

2.1. Single diode model

The structure of the single diode model is described as Fig. 1. In this model, the output current of the solar cell can be formulated as follows [39]:

$$I_C = I_{ph} - I_d - I_{sh} \quad (1)$$

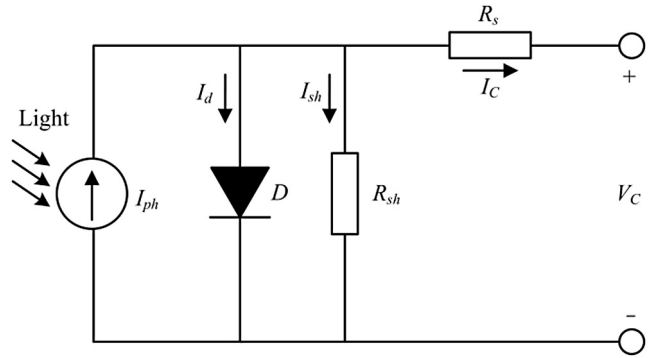


Fig. 1. The single diode model.

where I_C is the cell output current, I_{ph} is the photo generated current, I_d is the diode current, and I_{sh} is the shunt resistor current. According to the Shockley equation, I_d can be calculated as:

$$I_d = I_{sd} \left[\exp \left(\frac{q(V_C + I_C R_s)}{nkT} \right) - 1 \right] \quad (2)$$

where I_{sd} is the reverse saturation current of the diode, V_C is the cell output voltage, n is the diode ideality factor, R_s is the series resistance, k is the Boltzmann constant ($1.3806503 \times 10^{23} \text{ J/K}$), T is the temperature of the junction in Kelvin, and q is the electron charge ($1.60217646 \times 10^{-19} \text{ C}$).

Let $V_t = kT/q$, then Eq. (2) can be simplified as Eq. (3).

$$I_d = I_{sd} \left[\exp \left(\frac{V_C + I_C R_s}{nV_t} \right) - 1 \right] \quad (3)$$

The shunt resistor Current I_{sh} is formulated as:

$$I_{sh} = \frac{V_C + I_C R_s}{R_{sh}} \quad (4)$$

where R_{sh} is the shunt resistance.

Substituting Eqs. (3) and (4) into Eq. (1), the current-voltage relationship of the single diode model can be expressed as:

$$I_C = I_{ph} - I_{sd} \left[\exp \left(\frac{V_C + I_C R_s}{nV_t} \right) - 1 \right] - \frac{V_C + I_C R_s}{R_{sh}} \quad (5)$$

This model totally contains five parameters to be estimated (I_{ph} , I_{sd} , R_s , R_{sh} , and n).

2.2. Double diode model

The structure of the double diode model is described as Fig. 2. In this model, the cell output current I_C can be formulated as follows [39,40]:

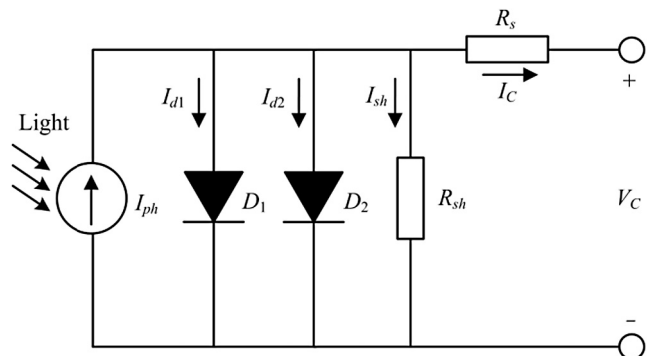


Fig. 2. The double diode model.

$$I_C = I_{ph} - I_{d1} - I_{d2} - I_{sh} \quad (6)$$

Similar with the single diode model, the current-voltage relationship of the double diode model can be finally expressed as:

$$\begin{aligned} I_C &= I_{ph} - I_{sd1} \left[\exp \left(\frac{V_C + I_C R_s}{n_1 V_t} \right) - 1 \right] \\ &\quad - I_{sd2} \left[\exp \left(\frac{V_C + I_C R_s}{n_2 V_t} \right) - 1 \right] - \frac{V_C + I_C R_s}{R_{sh}} \end{aligned} \quad (7)$$

Accordingly, this model totally contains seven parameters to be estimated (I_{ph} , I_{sd1} , I_{sd2} , R_s , R_{sh} , n_1 , and n_2).

2.3. PV module model

The single diode model and the double diode model of a PV module which consists of N_s connected cells in series can be also expressed as Eqs. (5) and (7), where $V_t = N_s kT/q$ [23,41].

2.4. Objective function

The estimation task aims to seek the most optimal values for the unknown parameters so as to minimize the error between the measured and simulated current. The root mean square of the error (RMSE) defined as Eq. (8) can be used as the objective function [23].

$$\text{RMSE}(X) = \sqrt{\frac{1}{N} \sum_{i=1}^N f(V_{Ci}, I_{Ci}, X)^2}, \quad (8)$$

where N is the number of the experimental data, X is the set of the estimated parameters.

For the single diode model, $f(V_C, I_C, X)$ and X can be respectively expressed as Eqs. (9) and (10).

$$f(V_C, I_C, X) = I_{ph} - I_{sd} \left[\exp \left(\frac{V_C + I_C R_s}{n V_t} \right) - 1 \right] - \frac{V_C + I_C R_s}{R_{sh}} - I_C \quad (9)$$

$$X = \{I_{ph}, I_{sd}, R_s, R_{sh}, n\} \quad (10)$$

For the double diode model, $f(V_C, I_C, X)$ and X can be respectively expressed as Eqs. (11) and (12).

$$\begin{aligned} f(V_C, I_C, X) &= I_{ph} - I_{sd1} \left[\exp \left(\frac{V_C + I_C R_s}{n_1 V_t} \right) - 1 \right] \\ &\quad - I_{sd2} \left[\exp \left(\frac{V_C + I_C R_s}{n_2 V_t} \right) - 1 \right] - \frac{V_C + I_C R_s}{R_{sh}} - I_C \end{aligned} \quad (11)$$

$$X = \{I_{ph}, I_{sd1}, I_{sd2}, R_s, R_{sh}, n_1, n_2\} \quad (12)$$

Obviously, smaller objective function value corresponds to better estimated parameters. Because of the objective function is non-linear and transcendental, this problem is difficult to solve.

3. The proposed hybrid algorithm

3.1. Basic flower pollination algorithm

Flower pollination algorithm is also a population-based algorithm which starts with a randomly generated candidate solution population. Then, FPA uses two different operators, i.e., the global search operator and the local search operator, to iteratively update the candidate solutions.

The global search operator is defined as Eq. (13) [31,32]:

$$x_i^{t+1} = x_i^t + \gamma s(x_i^t - g^*), \quad (13)$$

where x_i^t denotes the solution x_i at t -th iteration, g^* denotes the best solution in the current population, γ is a scale factor which controls

the step size, usually it is set to 0.01. s denotes the step size mimicked by a Lévy flight. In practice, s is usually generated using Metropolis algorithm as Eq. (14) [31,32], in which λ is generally set to 1.5.

$$s = \frac{U}{|V|^{1/\lambda}}, \quad U \sim N(0, \sigma^2), V \sim N(0, 1), \quad (14)$$

where U is a random number which fits a normal distribution with a mean of 0 and a variance of σ^2 which can be calculated as Eq. (15), where $\Gamma()$ denotes the standard gamma function, V is a random number which fits the standard normal distribution [31,32].

$$\sigma^2 = \left\{ \frac{\Gamma(1+\lambda)}{\lambda \Gamma[(1+\lambda)/2]} \cdot \frac{\sin(\pi\lambda/2)}{2^{(\lambda-1)/2}} \right\}^{1/\lambda} \quad (15)$$

The local search operator is defined as Eq. (16) [31,32]:

$$x_i^{t+1} = x_i^t + \varepsilon(x_j^t - x_k^t), \quad (16)$$

where x_j^t and x_k^t are two randomly selected solutions, ε is a uniform random number in [0,1].

Whether a newly generated candidate solution would be accepted is decided by a greedy strategy. If it is better than the old candidate solution, then the old one would be replaced by it, else, it would be given up.

FPA prefers the local search operator during the search process. A probability parameter p defined in the algorithm is used to achieve this. A suggested value of p is 0.8. This means that the local search operator would be selected with a probability of 0.8 while the global search operator would be selected with a probability of 0.2. More details about the FPA can be found in the literature [31,32].

3.2. Nelder-Mead simplex method

The Nelder-Mead simplex method (NM method) is specially designed for unconstrained minimization problems [42,43]. This method does not need the objective function's derivatives and has been widely used in many scientific and engineering problems [44–46].

The NM method is also an iterative algorithm. For a D dimensional minimization function, it starts from a simplex formed by $D+1$ initial vertices. In each iteration, some worst vertices would be replaced by newly generated vertices to obtain a new simplex. By constantly iteration, the simplex would be moved close to the optimal.

In detail, the NM method obeys the following steps in each iteration [42,43].

Step 1: Sort and number all the vertices in ascending order of their fitness function values, i.e., $f(X_1) \leq f(X_2) \leq f(X_3) \leq \dots \leq f(X_D) \leq f(X_{D+1})$;

Step 2: Calculate the reflection point X_r using Eq. (17) and its fitness function value $f(X_r)$. If $f(X_1) \leq f(X_r) < f(X_D)$, then replace X_{D+1} with X_r and go to Step 6; if $f(X_r) < f(X_1)$, then go to Step 3; if $f(X_r) \geq f(X_D)$, then go to Step 4;

$$X_r = (1 + \alpha) \cdot \bar{X} - \alpha \cdot X_{D+1}, \quad (17)$$

where α denotes the reflection factor, \bar{X} denotes the center of all the vertices except X_{D+1} calculated according to Eq. (18),

$$\bar{X} = \sum_{i=1}^n X_i / D \quad (18)$$

Step 3: Calculate the expansion point X_e using Eq. (19) and its fitness function value $f(X_e)$. If $f(X_e) \leq f(X_r)$, then replace X_{D+1} with X_e ; else, replace X_{D+1} with X_r . Then, go to Step 6.

$$X_e = (1 - \beta) \cdot \bar{X} + \beta \cdot X_r, \quad (19)$$

where β denotes the expansion factor.

Step 4: if $f(X_r) < f(X_{D+1})$, then calculate the outside contraction point X_{oc} using Eq. (20) and its fitness function value $f(X_{oc})$; else, calculate the inside contraction point X_{ic} using Eq. (21) and its fitness function value $f(X_{ic})$;

$$X_{oc} = (1 - \gamma) \cdot \bar{X} + \gamma \cdot X_r \quad (20)$$

$$X_{ic} = (1 - \gamma) \cdot \bar{X} + \gamma \cdot X_{D+1} \quad (21)$$

In Eqs. (20) and (21), γ denotes the contraction factor.

For the situation that X_{oc} is generated, if $f(X_{oc}) \leq f(X_r)$, then replace X_{D+1} with X_{oc} , and go to Step 6; else, go to Step 5. For the situation that X_{ic} is generated, if $f(X_{ic}) \leq f(X_{D+1})$, then replace X_{D+1} with X_{ic} , and go to Step 6; else, go to Step 5;

Step 5: shrinkage all the vertices except X_1 using Eq. (22) to get a new simplex, and go to Step 6.

$$V_i = \delta \cdot X_i + (1 - \delta) \cdot X_1, \quad \text{where } i = 2, \dots, D + 1, \quad (22)$$

where δ denotes the shrinkage factor.

Step 6: if the end condition is satisfied, end the search; else, go to the next iteration.

3.3. Generalized opposition-based learning mechanism

Opposition-based Learning (OBL), firstly proposed by Tizhoosh [47] and further illustrated in the literatures [48–54], has proven to be an effective approach for improving the performance of various meta-heuristic optimization algorithms. The basic idea of OBL is simultaneously evaluating the corresponding opposite population of the original candidate solution to increase the chance of finding better solutions [55].

The generalized opposition-based learning (GOBL) [56] is one of the most typical variants of the OBL. It has been successfully introduced into several heuristic algorithms to enhance their performances [57–59].

The opposite number and the opposite point are two basic concepts of OBL. The former is just suitable for one dimensional number, and the latter extends the former to higher dimensions.

Suppose that $x \in [a, b]$ is a real number, then its opposite number x^0 is defined as:

$$x^0 = a + b - x \quad (23)$$

Suppose that $X = (x_1, x_2, \dots, x_D)$ is a point in a D -dimensional space, where $x_j \in [a_j, b_j], j \in 1, 2, \dots, D$, its opposite point $X^0 = (x_1^0, x_2^0, \dots, x_D^0)$ is defined as:

$$x_j^0 = a_j + b_j - x_j, \quad \text{where } j = 1, 2, \dots, D \quad (24)$$

In GOBL, the opposite number and the opposite point are respectively extended to the generalized opposite number and the generalized opposite point respectively defined as Eqs. (25) and (26).

$$x^{GO} = k(a + b) - x, \quad (25)$$

$$x_j^{GO} = k(a + b) - x_j, \quad \text{where } j = 1, 2, \dots, D, \quad (26)$$

where k is a rand number within $[0, 1]$.

Comparing Eq. (23) with Eq. (25), it can be found that the opposite number is the symmetry point of the original number centered on the point $(a + b)/2$ and it is still located in the interval $[a, b]$, while the generalized opposite number is located in another interval $[k(a + b) - b, k(a + b) - a]$. Meanwhile, the generalized opposite number would degenerate to the opposite number when $k = 1$.

3.4. The proposed hybrid algorithm

The proposed algorithm in this study combines the basic FPA, the NM simplex method, and the GOBL mechanism together. The FPA is good at global exploration due to the Lévy flight, the NM simplex method is good at local search but highly susceptible to the initial points [44], the GOBL mechanism can help meta-heuristic algorithms jumping out of local optimum.

Firstly, the NM simplex method is introduced into the basic FPA to make intensive searches in the potential areas determined by the FPA. Detailedly, in each iteration, the algorithm firstly carries out the original operators of the basic FPA for the current population, and then switches to the NM simplex method. The best $D + 1$ solutions in the current population (here D denotes the number of the decision parameters) would be picked out and used to form an initial simplex. And then, the simplex would be updated using the NM simplex method for m iterations. Here m is an important parameter. If its value is too small, the local search ability of the NM method would not be exerted sufficiently. On the contrary, if its value is too large, the NM method would be overemphasized. By trial and error, its value is finally set to equal to $D + 1$. After the NM simplex method is executed for m iterations, the algorithm would be switched back to the FPA. The vertices of the updated simplex, together with the rest $N - (D + 1)$ solutions (here N represents the total number of candidate solutions) in the current population, are used to form the new population. The combination approach above is graphical described as Fig. 3.

During the execution of the NM simplex method part, if there are some newly generated solutions move out of the search space, the elements in these solutions would be restricted on the boundary which is nearer to them. Furthermore, in the shrinkage operator, the new obtained points would be compared with their corresponding vertices one to one. Only when the newly generated points are better they would be accepted, otherwise, the original vertices would be retained. According to our experiments, such a treatment could obtain better performance.

Then, the GOBL mechanism is incorporated. The GOBL part is located after the NM simplex method and executed with a given probability P_{GOBL} . This part works as follows. Suppose that the current population is $P(t)$ and it contains N candidate solutions as expressed by Eq. (27). Here t is the index of iterations. The generalized opposite population of $P(t)$ denoted as $GOP(t)$ would be calculated according to Eq. (28).

$$P(t) = \begin{bmatrix} X_1 \\ X_2 \\ \vdots \\ X_N \end{bmatrix} = \begin{bmatrix} x_{1,1} & x_{1,2} & \cdots & x_{1,D} \\ x_{2,1} & x_{2,2} & \cdots & x_{2,D} \\ \vdots & \vdots & \ddots & \vdots \\ x_{N,1} & x_{N,2} & \cdots & x_{N,D} \end{bmatrix} \quad (27)$$

$$GOP(t) = \begin{bmatrix} X_1^{GO} \\ X_2^{GO} \\ \vdots \\ X_N^{GO} \end{bmatrix} = \begin{bmatrix} x_{1,1}^{GO} & x_{1,2}^{GO} & \cdots & x_{1,D}^{GO} \\ x_{2,1}^{GO} & x_{2,2}^{GO} & \cdots & x_{2,D}^{GO} \\ \vdots & \vdots & \ddots & \vdots \\ x_{N,1}^{GO} & x_{N,2}^{GO} & \cdots & x_{N,D}^{GO} \end{bmatrix}, \quad (28)$$

$$\text{where } x_{ij}^{GO} = \begin{cases} k[a_j(t) + b_j(t)] - x_{ij}; \\ a_j(t) + \text{rand}(0, 1) \cdot (b_j(t) - a_j(t)), \\ \text{if } x_{ij}^{GO} < x_{min} \text{ or } x_{ij}^{GO} > x_{max} \end{cases}$$

where i denotes the index of the solutions in $P(t)$ ($i = 1, 2, \dots, N$), j denotes the index of the variables in each solution ($j = 1, 2, \dots, D$), $a_j(t) = \min(x_{ij})$ and $b_j(t) = \max(x_{ij})$ respectively denote the minimum and maximum values of the j -th dimensional variable in the current population, x_j^{\min} and x_j^{\max} respectively denote the inherent lower and upper boundaries of the j -th variable, $\text{rand}(0, 1)$ is a uni-

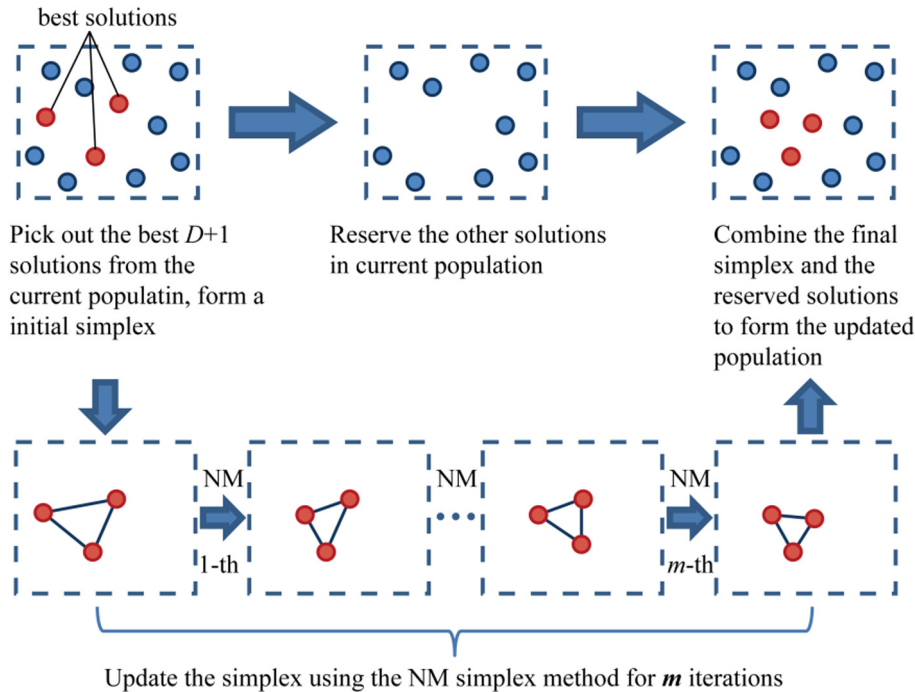


Fig. 3. The combination way of the NM method and the basic FPA.

form random number in $[0,1]$, k is also a uniform random number in $[0,1]$ and it is generated anew for every generalized opposite number. Here using the current reduced space ($a_j(t)$ and $b_j(t)$) rather than the inherent space to calculate the generalized opposite solution can fully make use of the knowledge obtained by the previous search process.

After that, the best N solutions among $\{P(t), \text{GOP}(t)\}$ would be used to replace the current population. Such an elite selection strategy can avoid the case that the generalized opposite solution may jump away from the global optimum.

The flowchart of the proposed hybrid algorithm is given in Fig. 4. It can be seen that its structure is relatively simple.

4. Experimental results and discussions

4.1. Test with the experimental data from Ref. [60]

To verify its performance, the proposed algorithm (GOFPANM, for short) is firstly tested on three parameters estimation problems taken from literature [60]. These problems include two cases of solar cells respectively corresponding to the single diode model and the double diode model and a case of the PV module. Meanwhile, the basic flower pollination algorithm (BFPA), the flower pollination algorithm only combined with the OBL (OFPA), the flower pollination algorithm only combined with the GOBL (GOFPA), the flower pollination algorithm only combined with the NM simplex method (BFPANM), and the flower pollination algorithm simultaneously combined with the OBL and the NM simplex method (OFPANM) are simultaneously tested on these three cases. The OBL part or the NM simplex method part involved in the OFPA, the GOFPA, the BFPANM, the OFPANM, and the GOFPANM are combined with the basic FPA in the same ways involved in the GOFPANM. Furthermore, to demonstrate the superiority of the proposed algorithm, its results are compared with those of some recently published methods.

All the six algorithms are implemented in MATLAB R2012a. The following parameters are used in the experiments and the common

parameters involved in the six algorithms are set to same. The population size N is set to 10. The switch probability p is set to 0.8. The parameters of the NM method part are set according to the standard setting, i.e., the reflection factor α is 1, the expansion factor β is 2, and both the contraction factor γ and the shrinkage factor δ are 0.5. The P_{GOBL} (P_{OBL} in the OFPA and the OFPANM) is set to 0.15 for the single and the double diode model, and 0.4 for the PV module by trial and error. The parameters search ranges are listed in Table 1. For every case, every algorithm is tested 30 independent runs. The maximum number of function evaluations (MAX_NFFE) which is set to 10,000 for the single diode model solar cell case and the PV module case and 20,000 for the double diode mode case is used as the terminal condition of every run. The experimental $I-V$ dataset of the two cases of the solar cell are measured from a 57 mm diameter commercial RTC France silicon solar cell at an irradiance of (1000 W/m^2) and a temperature of (33°C) and totally contains 26 pairs of current and voltage values. The experimental $I-V$ dataset for the case of the PV module are measured from a Photo watt-PWP 201 PV module in which 36 polycrystalline silicon cells are connected in series at an irradiance of (1000 W/m^2) and a temperature of (45°C) , and totally contains 25 pairs of current and voltage values [60].

The following four performance criteria are adopted to comprehensively compare the performance of the six tested algorithms [12,23].

RMSE: As expressed in Eq. (8), it is used to measure the quality of the solutions finally obtained by an algorithm.

NFFEs^{*}: NFFEs^{*} denotes the number of fitness function evaluations in each run for finding a solution whose fitness function value is less than VTR, where VTR is a very small positive value pre-defined. NFFEs^{*} is used to measure the convergence speed of an algorithm.

Success rate (SR): the run in which the algorithm finally obtained a solution whose fitness function value is less than VTR is regarded as a successful run. SR is calculated as the number of successful runs divided by the total number of runs and it is used to measure the reliability of an algorithm.

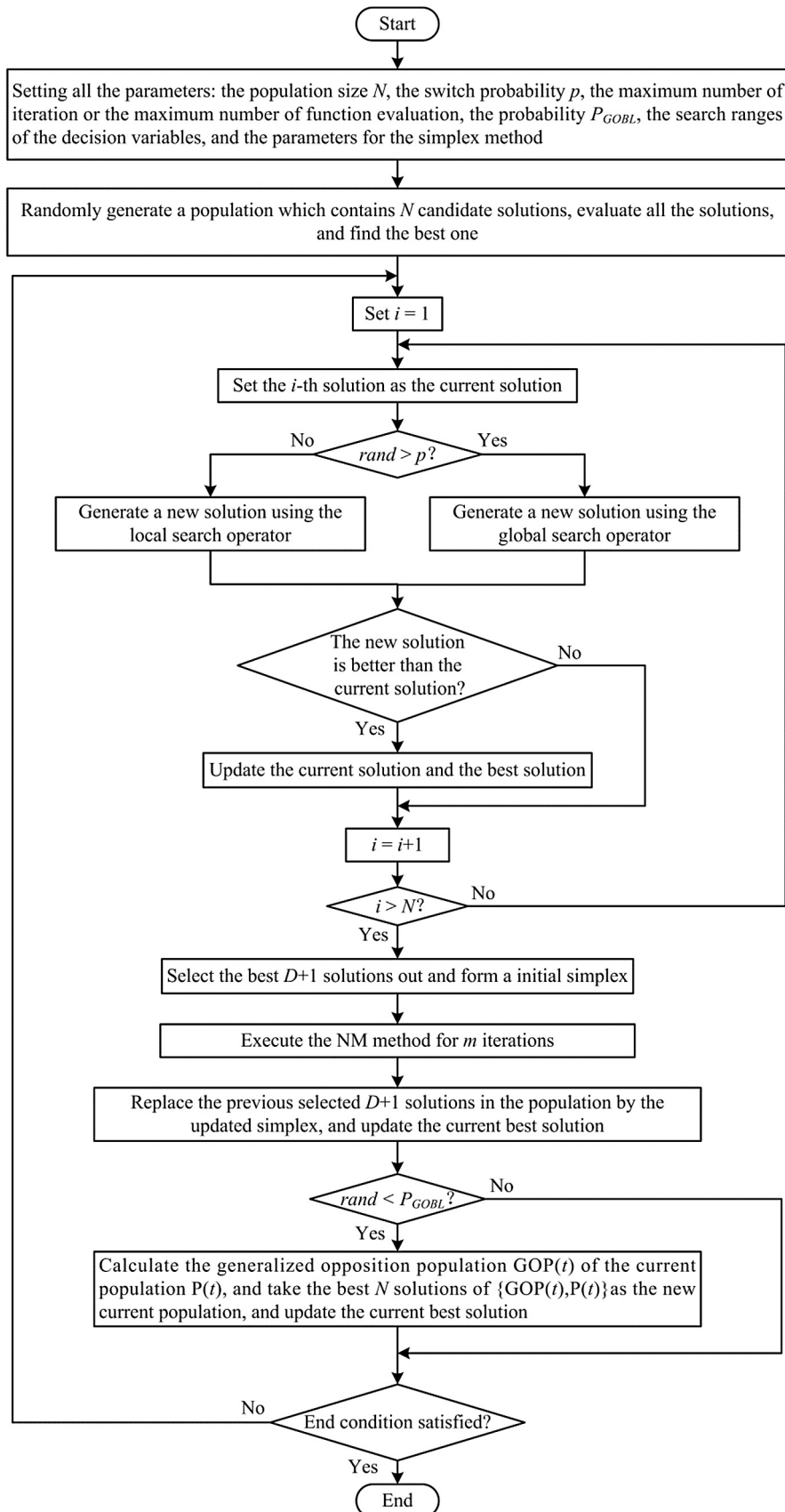


Fig. 4. Flowchart of the proposed algorithm.

Table 1

Parameters search ranges of the single and double diode models for RTC France solar cell and Photo watt-PWP 201 PV module.

Parameter	Cases of solar cells		PV module	
	Lower bound	Upper bound	Lower bound	Upper bound
I_{ph} (A)	0	1	0	2
I_{sd} (μ A)	0	1	0	50
R_s (Ω)	0	0.5	0	2
R_{sh} (Ω)	0	100	10	2000
n	1	2	0	50

Convergence graphs: Convergence graphs are used to show the mean RMSE performance of the best solution over the total number of runs.

4.1.1. Results on the single diode model case

For the single diode model case, the comparisons of the six tested algorithms on the RMSE, the NFFE s^* , and the SR are arranged in Table 2, in which the best results have been marked in bold. The convergence graphs of them are given in Fig. 5. Furthermore, the comparisons between the I - V characteristics and the power vs. voltage (P - V) characteristics of the best model estimated by the GOFPANM and the experimental data are given in Fig. 6. Meanwhile, two indexes respectively named as individual absolute error (IAE) and relative error (RE) and respectively defined as Eqs. (29) and (30) are adopted to indicate the error values between the experimental and the simulated current data, as showed in Fig. 7.

$$\text{IAE} = |I_{\text{measured}} - I_{\text{estimated}}| \quad (29)$$

$$\text{RE} = (I_{\text{measured}} - I_{\text{estimated}})/I_{\text{measured}} \quad (30)$$

From Table 2, it can be seen that, for the single diode model case, the best RMSE values obtained by the BFPA, the GOFPA, the BFPANM, the OFPANM, and the GOFPANM are same (9.8602E-04), while that obtained by the OPFA are slightly worse (9.864331E-04). Considering the other terms, the OFPANM performs best among the six tested algorithms, followed by the GOFPANM. On the whole, the GOFPANM can still be regarded as comparable with the OFPANM though it slightly lags behind the GOFPANM on the stand deviation of the RMSE values and the terms of the NFFE s^* . Both these two algorithms are reliable enough.

From Fig. 5, it can be seen that, the GOFPANM and the OFPANM show superiority than the other algorithms on the convergence speed. After about 5000 times of fitness function evaluations, these two algorithms have almost reached the final values.

From Figs. 6 and 7, it can be seen that the I - V curve and the P - V curve of the estimated model are quite consistent with the experimental data over the whole voltage range. All the IAE values are smaller than 1.6E-3 and all the RE values fall within the interval [-1.5E-2, 8E-2]. This indicates that the actual behavior of the solar cell can be accurately described by the single diode model estimated by the GOFPANM.

Furthermore, the best results obtained by the GOFPANM for this case are compared with those of CPSO [18], PS [1], LMSA [61], IGHS

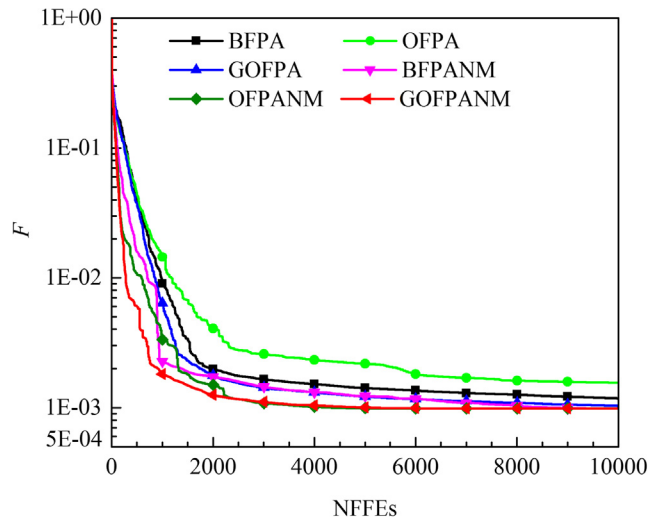


Fig. 5. Convergence graphs of the six algorithms for RTC France solar cell (single diode model).

[24], ABC [26], ABSO [15], BBO-M [11], and GOTLBO [12], as arranged in Table 3. It can be clearly found that the results of the GOFPANM are better than those of the other algorithms, though some algorithms such as the IGHS, ABC, ABSO, BBO-M cost more number of fitness function evaluations. This indicates that the GOFPANM is more effective.

4.1.2. Results on the double diode model case

For this case, the RMSE, the NFFE s^* , and the SR of the six tested algorithms are arranged in Table 4, and their convergence graphs are given in Fig. 8. The I - V characteristics and the P - V characteristics of the best model estimated by the GOFPANM and the experimental data are given in Fig. 9. The IAE and the RE values are showed in Fig. 10.

From Table 4, it can be seen that, for this case, the best RMSE values obtained by the BFPANM, the OFPANM, and the GOFPANM are same (9.824849E-04) and better than those obtained by the other three algorithms. Taking the OFPANM and the GOFPANM into comparison, the former performs better on the median value of RMSE and the mean value of NFFE s^* while the latter performs

Table 2

The statistical results obtained by the BFPA, OFPA, GOFPA, BFPANM, OFPANM, and GOFPANM for RTC France solar cell (single diode model).

Algorithm	RMSE					NFFE s^* (VTR = 0.001)		SR
	Min	Mean	Median	Max	Std	Mean	Std	
BFPA	9.860219E-04	1.181243E-03	1.133753E-03	1.943194E-03	2.419249E-04	6.3661E+03	2.3225E+03	12/30
OPFA	9.864331E-04	1.555484E-03	1.295447E-03	6.724120E-03	1.021888E-03	1305	NA	1/30
GOFPA	9.860219E-04	1.032412E-03	1.008452E-03	1.242476E-03	6.001251E-05	6.6326E+03	2.4119E+03	12/30
BFPANM	9.860219E-04	9.873385E-04	9.860219E-04	1.025520E-03	7.211294E-06	3.1983E+03	2.1512E+03	29/30
OFPANM	9.860219E-04	9.860219E-04	9.860219E-04	9.860219E-04	3.385613E-16	2.9038E+03	996.2544	30/30
GOFPANM	9.860219E-04	9.860219E-04	9.860219E-04	9.860219E-04	5.591415E-15	3.1638E+03	1.5580E+03	30/30

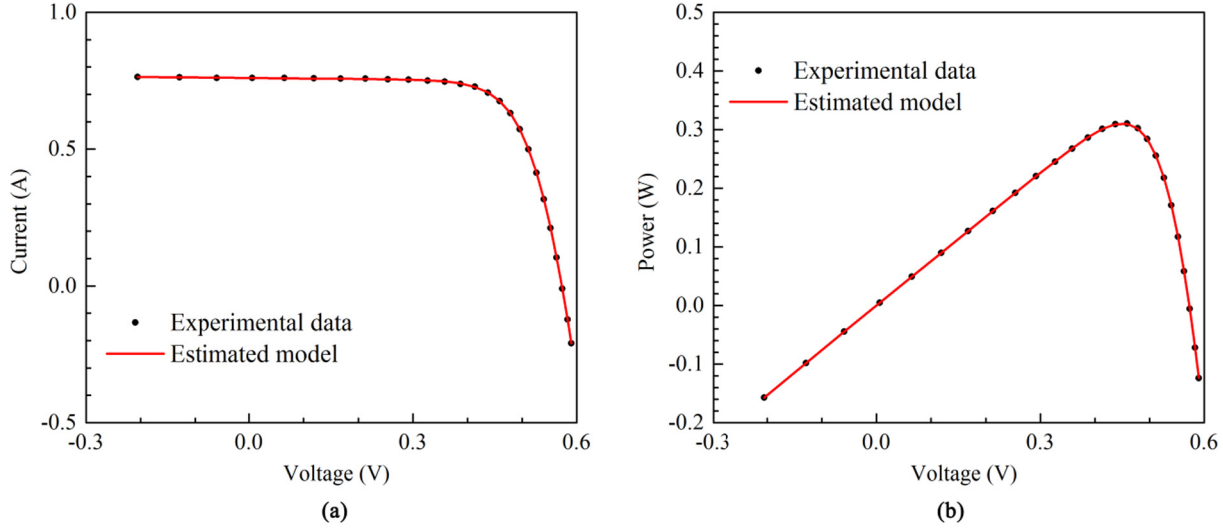


Fig. 6. Comparisons of the characteristics of the estimated model and the experimental data of RTC France solar cell (single diode model) (a) I - V characteristics; (b) P - V characteristics.

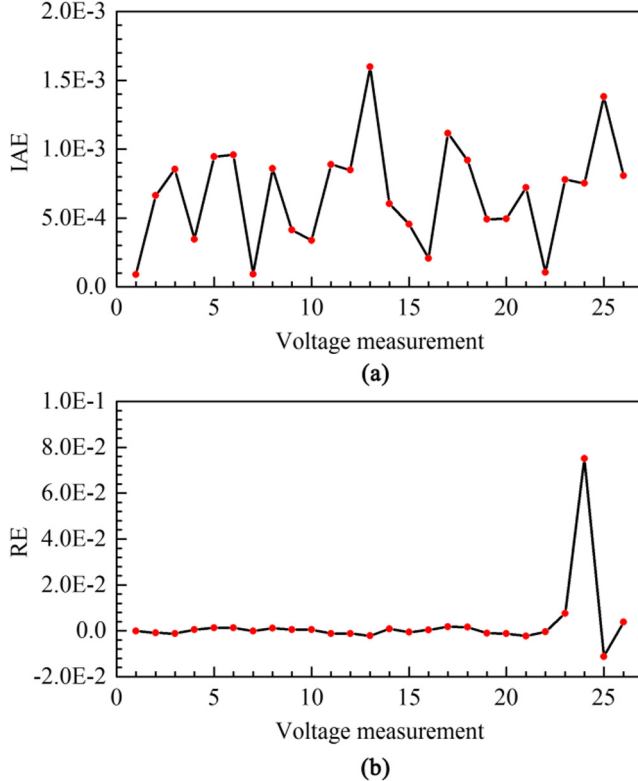


Fig. 7. Error index values of the simulated current data and the experimental current data of RTC France solar cell (single diode model) (a) IAE values; (b) RE values.

better on the mean and maximum value and the standard deviation of the RMSE, the standard deviation of the NFFE*, and the SR.

From Fig. 8, it can be clearly seen that, the GOFPANM and the BFPANM converge faster than the other algorithms. The GOFPANM has almost reached the final result after about 5000 times of fitness function evaluations, and the BFPANM has almost reached the final result after about 8000 times of fitness function evaluations.

From Figs. 9 and 10, it can be found that the estimated double diode model also can accurately describe the actual behavior of the solar cell. As similar as showed on the single diode model case, the I - V curve and the P - V curve of the estimated model are also quite consistent with the experimental data. All the IAE values are smaller than $1.5E-3$ and all the RE values fall within the interval $[-1.5E-2, 8E-2]$.

The best estimated parameters of the GOFPANM for this case are compared with those of PS [1], SA [62], IGHS [24], ABC [26], ABSO [15], STLBO [9], and BBO-M [11], as arranged in Table 5. From this table, it can be found that, only the results of the STLBO are comparative with the results of the GOFPANM and those of the other algorithms are obviously worse. However, the NFFE* (50,000) cost by the STLBO are much more than that cost by the GOFPANM (20,000).

4.1.3. Results on the PV module case

For this case, the RMSE, the NFFE*, and the SR of the six tested algorithms are arranged in Table 6, and the convergence graphs of them are given in Fig. 11. Similarly, the best results in Table 6 have been marked in bold. The I - V characteristics and the P - V characteristics of the best model estimated by the GOFPANM and the experimental data are given in Fig. 12. The IAE and the RE values are showed in Fig. 13.

Table 3

Comparison of GOFPANM with other published methods for RTC France solar cell (single diode model).

Item	CPSO	PS	LMSA	IGHS	ABC	ABSO	GOTLBO	BBO-M	GOFPANM
I_{ph} (A)	0.7607	0.7617	0.76078	0.7608	0.7608	0.7608	0.76078	0.76078	0.7607755
I_{sd} (μ A)	0.4	0.998	0.31849	0.3435	0.3251	0.30623	0.331552	0.31874	0.3230208
R_s (Ω)	0.0354	0.0313	0.03643	0.0361	0.0364	0.03659	0.036265	0.03642	0.0363771
R_{sh} (Ω)	59.012	64.1026	53.32644	53.2845	53.6433	52.2903	54.11543	53.36227	53.7185203
n	1.5033	1.6	1.47976	1.4874	1.4817	1.47878	1.48382	1.47984	1.4811836
RMSE	1.3900E-03	1.4940E-02	9.8640E-4	9.9306E-04	9.862E-04	9.9124E-04	9.87442E-04	9.8634E-04	9.8602E-04
NFES	45,000	NA	NA	150,000	1,500,000	150,000	10,000	80,000	10,000

Table 4

The statistical results obtained by the BFPA, OFPA, GOFPA, BFPANM, OFPANM, and GOFPANM for RTC France solar cell (double diode model).

Algorithm	RMSE					NFFEs* (VTR = 0.001)		SR
	Min	Mean	Median	Max	Std	Mean	Std	
BFPA	9.835164E-04	1.137981E-03	1.000178E-03	1.934336E-03	2.440882E-04	7.2885E+03	2.0475E+03	4/30
OFPA	9.824880E-04	1.126655E-03	1.013873E-03	2.694986E-03	3.260462E-04	6.9057E+03	2.2433E+03	7/30
GOFPA	9.828786E-04	1.086296E-03	9.954871E-04	2.062861E-03	2.189113E-04	6.9925E+03	3.7908E+03	2/30
BFPANM	9.824849E-04	1.033001E-03	9.824883E-04	2.448049E-03	2.672921E-04	3.2694E+03	1.8670E+03	28/30
OFPANM	9.824849E-04	1.032070E-03	9.824849E-04	2.448049E-03	2.674390E-04	3.1820E+03	1.7888E+03	28/30
GOFPANM	9.824849E-04	9.954827E-04	9.827174E-04	1.340531E-03	6.518742E-05	3.2590E+03	1.6901E+03	29/30

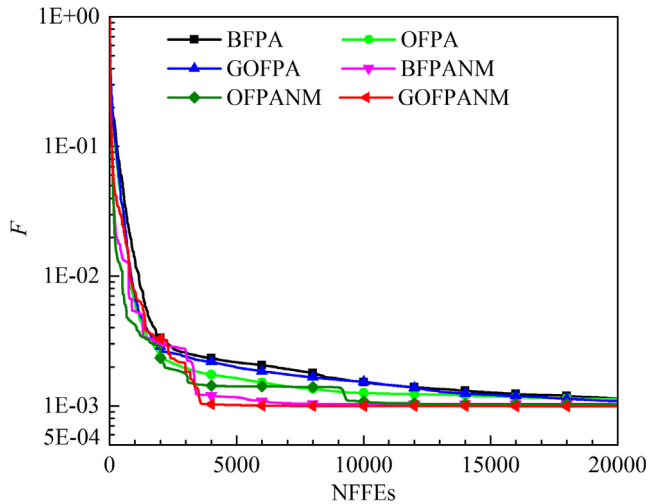


Fig. 8. Convergence graphs of the six algorithms for RTC France solar cell (double diode model).

From Table 6, it can be clearly seen that, the best RMSE values obtained by the BFPA, the GOFPA, the BFPANM, the OFPANM, and the GOFPANM are same (2.425075E-03) and slightly better than that obtained by the OFPA (2.432568E-03). Meanwhile, the GOFPANM surpass the other algorithms on the comparisons of all the other terms, indicating that the GOFPANM has better stability, reliability, and faster convergence speed.

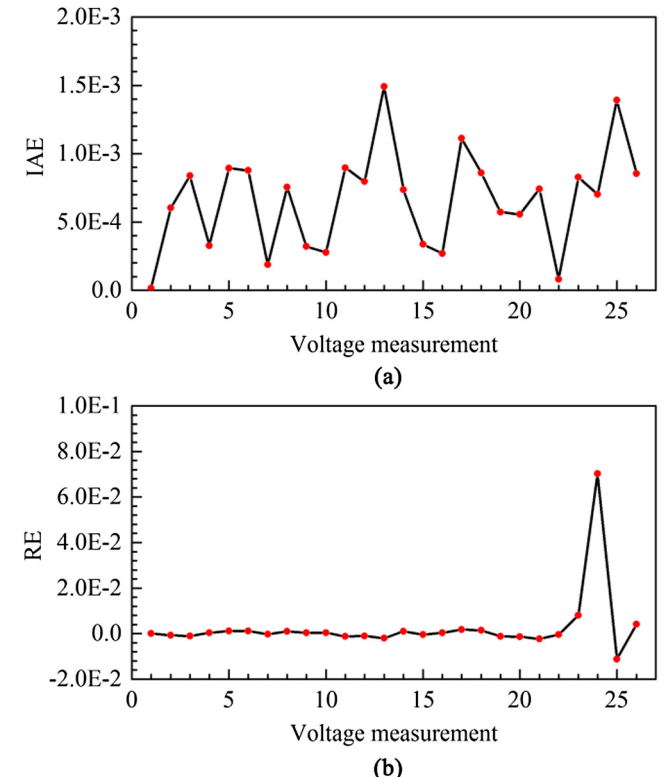


Fig. 10. Error index values of the simulated current data and the experimental current data of RTC France solar cell (double diode model) (a) IAE values; (b) RE values.

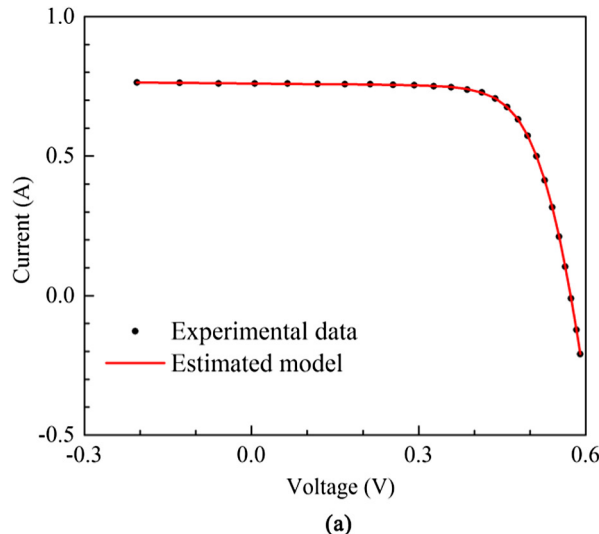


Fig. 9. Comparisons of the characteristics of the estimated model and the experimental data of RTC France solar cell (double diode model) (a) I - V characteristics; (b) P - V characteristics.

Table 5

Comparison of GOFPANM with other published methods for RTC France solar cell (double diode model).

Item	PS	SA	IGHS	ABC	ABSO	STLBO	GOTLBO	BBO-M	GOFPANM
I_{ph} (A)	0.7602	0.7623	0.7608	0.7608	0.76077	0.76078	0.760752	0.76083	0.7607811
I_{sd1} (μ A)	0.9889	0.4767	0.9731	0.0407	0.26713	0.22566	0.800195	0.59115	0.7493476
I_{sd2} (μ A)	0.0001	0.01	0.1679	0.2874	0.38191	0.75217	0.220462	0.24523	0.2259743
R_s (Ω)	0.032	0.0345	0.0369	0.0364	0.03657	0.03674	0.036783	0.03664	0.0367404
R_{sh} (Ω)	81.3008	43.1034	53.8368	53.7804	54.6219	55.492	56.0753	55.0494	55.4854485
n_1	1.6	1.5172	1.9213	1.4495	1.46512	1.45085	1.999973	2.00000	2.00000
n_2	1.192	2	1.4281	1.4885	1.98152	2	1.448974	1.45798	1.4510168
RMSE	1.5180E-02	1.6640E-02	9.8635E-04	9.861E-04	9.8344E-04	9.8248E-04	9.83177E-04	9.8272E-04	9.8248E-04
NFES	NA	NA	150,000	1,500,000	150,000	50,000	20,000	80,000	20,000

Table 6

The statistical results obtained by the BFPA, OFPA, GOFPA, BFPANM, OFPANM, and GOFPANM for Photo watt-PWP 201 PV module (single diode model).

Algorithm	RMSE					NFFEs [*] (VTR = 0.01)		SR
	Min	Mean	Median	Max	Std	Mean	Std	
BFPA	2.425075E-03	1.370372E-02	2.436494E-03	2.742508E-01	5.034340E-02	2.2295E+03	2.3727E+03	28/30
OFPA	2.432568E-03	7.746727E-02	5.096233E-03	3.916690E-01	1.316078E-01	1.5263E+03	2.2038E+03	18/30
GOFPA	2.425075E-03	2.462837E-03	2.425255E-03	3.075790E-03	1.263460E-04	1.1666E+03	586.7744	30/30
BFPANM	2.425075E-03	1.164947E-02	2.425075E-03	2.742508E-01	4.960239E-02	1.5980E+03	2.2232E+03	29/30
OFPANM	2.425075E-03	2.961669E-02	2.425075E-03	2.742508E-01	8.293873E-02	895.4815	896.4294	27/30
GOFPANM	2.425075E-03	2.425075E-03	2.425075E-03	2.425075E-03	2.918886E-16	812.1333	744.7365	30/30

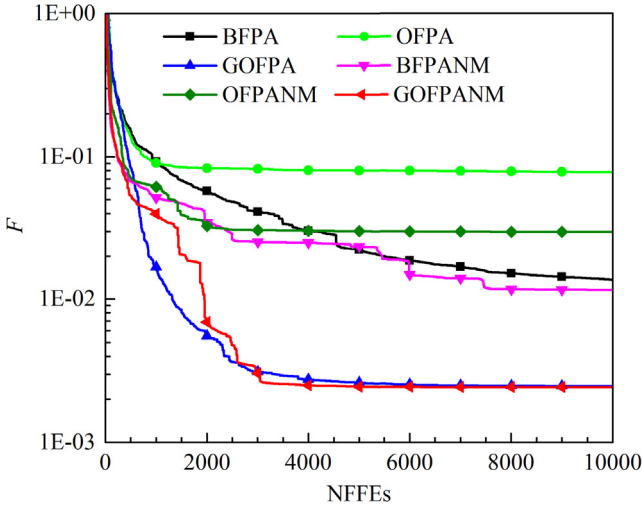


Fig. 11. Convergence graphs of the six algorithms for Photo watt-PWP 201 PV module (single diode model).

From Fig. 11, it can be seen that, for this case, the average convergence speed of the GOFPANM and the GOFPA are significantly faster than the other four algorithms. This is mainly because the other four algorithms are more easily trapped in local optimal, as that indicated in the previous comparison of the SR. Meanwhile, the GOFPANM converges slightly faster than the GOFPA. After about 4000 times of fitness function evaluations, the GOFPANM has almost reached the final result while the same situation of the BFPANM appears after about 6000 times of fitness function evaluations.

From Figs. 12 and 13, it can be found that for this case, the accuracy of the estimated model is also satisfactory. The I - V curve and the P - V curve of the estimated model are also in quite good agreement with the experimental data. All the IAE values are smaller than $4.5E-3$ and all the RE values fall within the interval $[-2.5E-2, 3E-2]$.

The best results of the GOFPANM for this case are compared with those of the Newton method [60], the CPSO [18], the method

in [63], the method in [64], the PS [1], the SA [62], and the R_{cr} -IJADE [23], as showed in Table 7. From this table, it can be found that only the results of the R_{cr} -IJADE are comparative with the results of the GOFPANM and those of the other methods are obviously worse. There is only a slight difference between the results of the R_{sh} obtained by the R_{cr} -IJADE and the GOFPANM. What needs to be stressed is that the R_{cr} -IJADE is the most excellent one among various reported methods. Meanwhile, some methods listed in this table have several additional limitations. For example, the Newton method requires differentiability condition and involves heavy computations, the PS and the SA are highly dependent on the initial values of the parameters to be estimated thus the start solutions should be elaborately selected, and the methods given in [63,64] involve tedious theoretical analysis. The GOFPANM doesn't have these limitations. As a variant of the flower pollination algorithm, it only requires a coarse search range for every parameter thus the estimation procedure can be significantly simplified.

By comprehensively comparing their performances showed on the three tested cases, it can be found that the GOFPANM is best among the six tested algorithms. Meanwhile, due to its superiority shown in the comparisons with the other recently published methods, the GOFPANM can be regarded as a new and effective method for the parameter estimation problems of the solar cells/PV modules.

4.2. Tests with experimental data from the manufacturer's data sheet

To further examine its practicability, in this section, the proposed algorithm is used to extract the optimal parameters of both the single diode and double diode models for three solar modules of different types (Multi-crystalline (S75 [65]), Thin-film (ST40 [66]), and Mono-crystalline (SM55 [67])). The experimental data is directly extract from the (I - V) curves given in the manufacturer's data sheets at five different irradiance levels i.e. 1000 W/m^2 , 800 W/m^2 , 600 W/m^2 , 400 W/m^2 , and 200 W/m^2 , and three temperature levels.

In this part, The population is set to 20, the maximum number of function evaluations is set to 10,000. The other parameters are set as same as those used in the previous PV module case.

The search range of I_{ph} is determined based on the data sheet parameters of each module at Standard Test Conditions (STC):

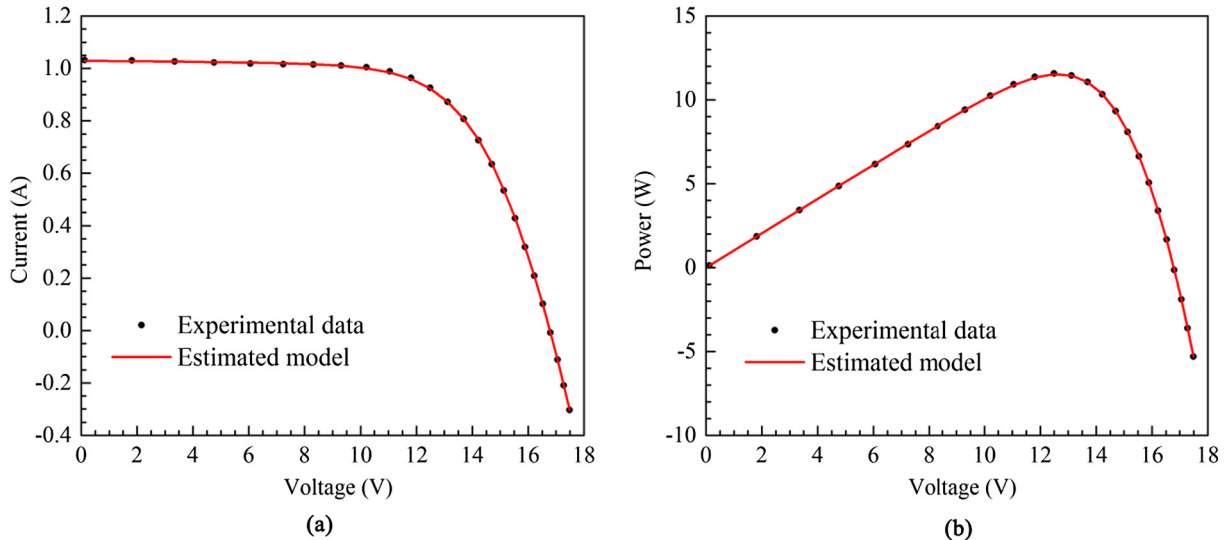


Fig. 12. Comparisons of the characteristics of the estimated model and the experimental data of Photo watt-PWP 201 PV module (single diode model) (a) I - V characteristics; (b) P - V characteristics.

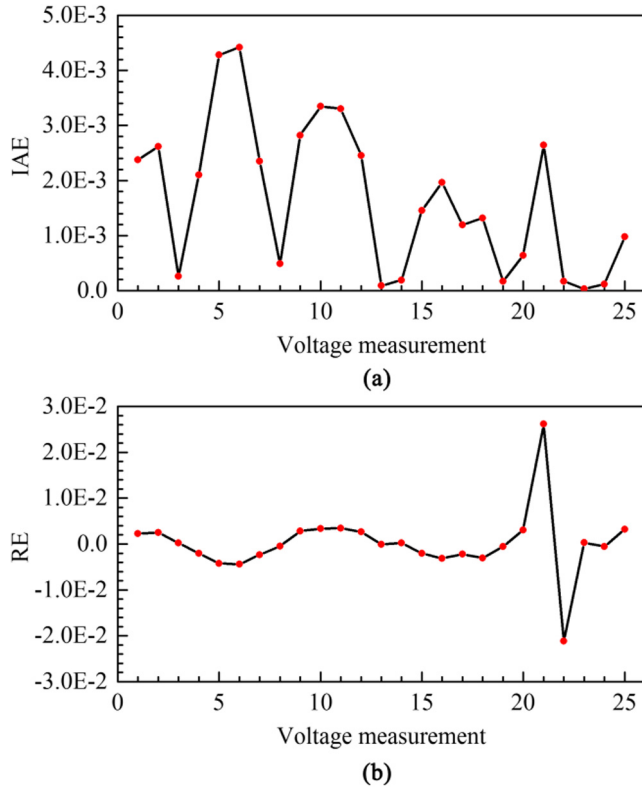


Fig. 13. Error index values of the simulated current data and the experimental current data of Photo watt-PWP 201 PV module (single diode model) (a) IAE values; (b) RE values.

short circuit current I_{SC_STC} , temperature coefficient for short circuit current α [38]. Firstly, the I_{SC} at non-standard conditions are calculated as Eq. (31).

$$I_{SC}(G, T) = I_{SC_STC} * \frac{G}{G_{STC}} + \alpha(T - T_{STC}), \quad (31)$$

where G and T denote irradiance and temperature, respectively.

Then, the search range of I_{ph} is set as $I_{ph} \in [0, 2I_{SC}]$ (A), the search ranges of other parameters are set as $I_{sd} \in [0, 1]$ (μ A), $R_s \in [0, 2]$ (Ω), $R_{sh} \in [0, 5000]$ (Ω) and $n \in [1, 4]$.

4.2.1. Case study 1: single diode model

The optimal parameters of the single diode model extracted for the three solar modules at different temperature values are given in Tables 8–10. Meanwhile, the optimal parameters extracted for them at different irradiance levels are given in Table 11. The comparisons between the estimated models and the experimental data

Table 8

The extracted parameters for Multi-crystalline S75 PV module by GOFPANM at different temperature and irradiance of 1000 W/m^2 (single diode model).

Parameters	Temperature		
	(25 °C)	(50 °C)	(60 °C)
Multi-crystalline S75			
I_{ph} (A)	4.69672364	4.74017858	4.76427536
I_{sd} (μ A)	0.02417760	1.00000000	1.00000000
R_s (Ω)	0.25970541	0.28811186	0.33253685
R_{sh} (Ω)	373.18721829	588.98453712	392.52478103
n	1.22190338	1.28514410	1.20206778
RMSE	0.02532146	0.02873236	0.03827746

Table 7

Comparison of GOFPANM with other published methods for Photo watt-PWP 201 PV module (single diode model).

Item	Newton	Method in [63]	CPSO	Method in [64]	PS	SA	R_{cr} -IJADE	GOFPANM
I_{ph} (A)	1.0318	1.0339	1.0286	1.0310	1.0313	1.0331	1.030514	1.0305143
I_{sd} (μ A)	3.2875	3.0760	8.3010	3.8236	3.1756	3.6642	3.482263	3.4822631
R_s (Ω)	1.2057	1.2030	1.0755	1.0920	1.2053	1.1989	1.201271	1.2012710
R_{sh} (Ω)	555.5556	555.5556	1850.1000	689.6600	714.2857	833.3333	981.982240	981.982240
n	48.4500	48.1862	52.2430	48.9300	48.2889	48.8211	48.642835	48.6428351
F	0.7805	0.6130	0.0035	0.0102	0.0118	0.0027	0.002425	0.002425
NFFEs	NA	NA	NA	NA	NA	NA	10,000	10,000

Table 9

The extracted parameters for Thin-film ST40 PV module by GOFPANM at different temperature and irradiance of 1000 W/m² (single diode model).

Parameters	Temperature		
	(25 °C)	(40 °C)	(50 °C)
Thin-film ST40			
I_{ph} (A)	2.70190621	2.74449554	2.76724722
I_{sd} (μ A)	0.08247954	1.00000000	1.00000000
R_s (Ω)	1.29027070	1.19126284	1.28862020
R_{sh} (Ω)	223.41992758	146.05998498	120.25993697
n	1.25470413	1.30342598	1.20767173
RMSE	0.01883885	0.01749461	0.01963535

Table 10

The extracted parameters for Mono-crystalline SM55 module by GOFPANM at different temperature and 25 °C (single diode model).

Parameters	Temperature		
	(25 °C)	(40 °C)	(60 °C)
Multi-crystalline SM55			
I_{ph} (A)	3.40353918	3.41575661	3.44097942
I_{sd} (μ A)	0.00122095	0.01737744	0.38612572
R_s (Ω)	0.47711982	0.48226924	0.46886296
R_{sh} (Ω)	455.66373078	625.75459889	1113.69240439
n	1.08027562	1.11277268	1.15546360
RMSE	0.01464569	0.01080231	0.00983344

Table 11

The extracted parameters for three different types of PV modules by GOFPANM at different radiation and 25 °C (single diode model).

Parameters	Multi-crystalline S75	Thin-film ST40	Mono-crystalline SM55
$G = 1000 \text{ W/m}^2$			
I_{ph} (A)	4.69672364	2.70190621	3.40353918
I_{sd} (μ A)	0.02417760	0.08247954	0.00122095
R_s (Ω)	0.25970541	1.29027070	0.47711982
R_{sh} (Ω)	373.18721829	223.41992758	455.66373078
n	1.22190338	1.25470413	1.08027562
RMSE	0.02532146	0.01883885	0.01464569
$G = 800 \text{ W/m}^2$			
I_{ph} (A)	3.75878440	2.16798184	2.72575491
I_{sd} (μ A)	0.00162921	1.00000000	0.00061643
R_s (Ω)	0.36715949	1.09961487	0.53558650
R_{sh} (Ω)	373.75886594	194.62100715	423.98706670
n	1.07096888	1.45928972	1.04781702
RMSE	0.02054906	0.01454162	0.02481861
$G = 600 \text{ W/m}^2$			
I_{ph} (A)	2.82486788	1.62243874	2.04753928
I_{sd} (μ A)	0.00035256	1.00000000	0.00895816
R_s (Ω)	0.41034479	1.20556691	0.44009140
R_{sh} (Ω)	318.37639750	264.74198273	471.55955541
n	1.00000172	1.45563886	1.18931250
RMSE	0.02275590	0.01251004	0.01117803
$G = 400 \text{ W/m}^2$			
I_{ph} (A)	1.88430086	1.08335493	1.35851636
I_{sd} (μ A)	0.00616669	1.00000000	0.08548610
R_s (Ω)	0.26580477	1.32086365	0.27018628
R_{sh} (Ω)	349.13038614	310.22804043	1056.32747008
n	1.13878695	1.45166828	1.34941540
RMSE	0.00933448	0.00787280	0.00605317
$G = 200 \text{ W/m}^2$			
I_{ph} (A)	0.94388136	0.54629683	0.69407321
I_{sd} (μ A)	0.03249028	1.00000000	0.00229907
R_s (Ω)	0.20865642	2.00000000	0.65879480
R_{sh} (Ω)	415.34685178	343.37457903	288.05490915
n	1.25157503	1.43716017	1.10530209
RMSE	0.00162572	0.00768238	0.00251129

of the three PV modules at different temperature values are given in Figs. 14–16 and at different irradiance levels are given in Figs. 17–19.

It can be observed that, for all the three PV modules, the I-V curves of the estimated single diode models strongly agree to the experimental data at all irradiance levels and temperature values under investigation. In particular, at low irradiance level which is very crucial when the module is subjected to certain mismatch conditions such as partial shading, the estimated models are also very accurate.

From Tables 8–11, it can be found that, the values of the series resistance R_s falls within the interval [1,2] for Thin-film ST40 and is less than 0.7 for both Multi-crystalline S75 and Mono-crystalline SM55. Usually, in PV module, series resistance R_s is found to be very low while parallel resistance R_{sh} is very high. The extracted results in this study agree with this point.

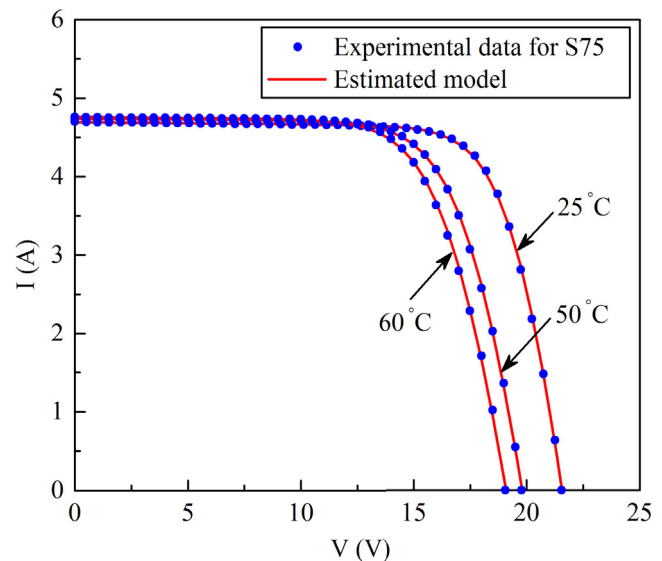


Fig. 14. Comparison between the estimated model and the experimental data of Multi-crystalline S75 at different temperature (single diode model).

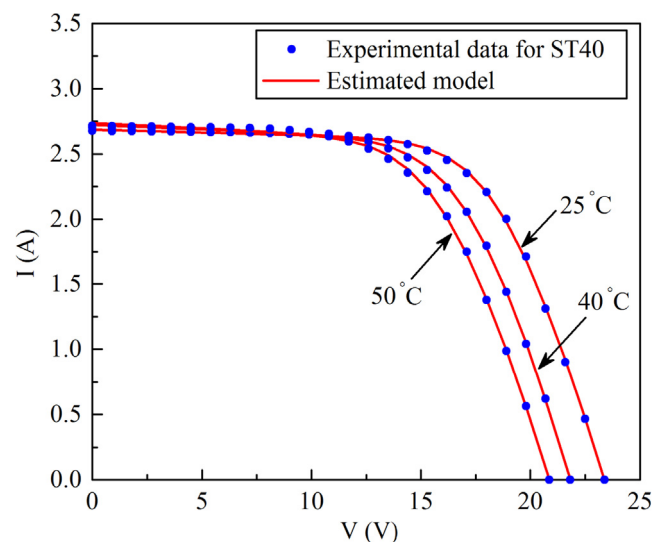


Fig. 15. Comparison between the estimated model and the experimental data of Thin-film ST40 at different temperature (single diode model).

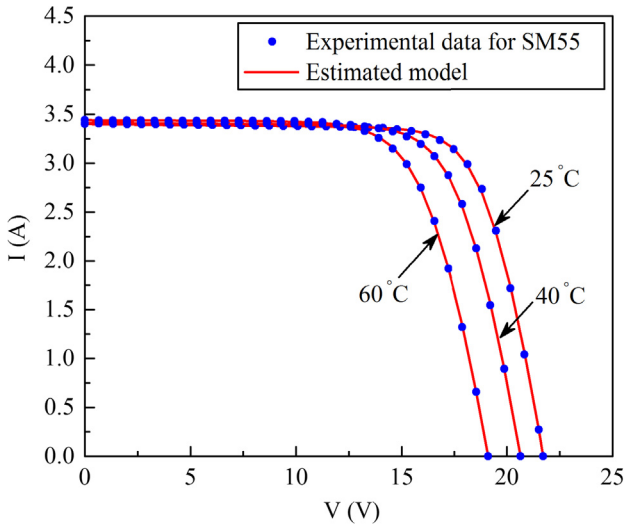


Fig. 16. Comparison between the estimated model and the experimental data of Mono-crystalline SM55 at different temperature (single diode model).

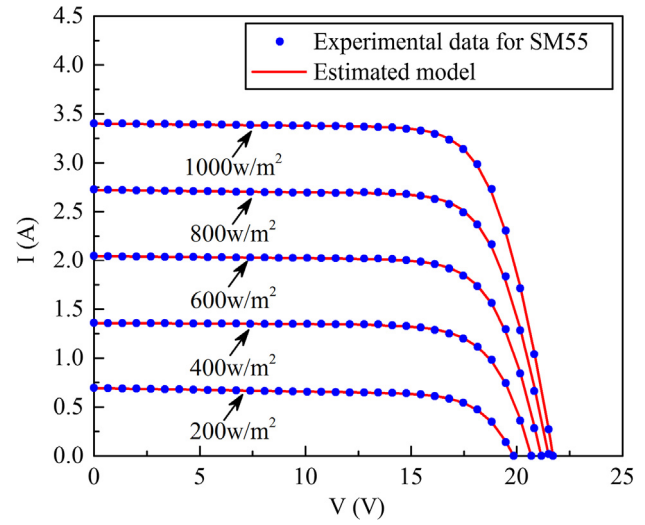


Fig. 19. Comparison between the estimated model and the experimental data of Mono-crystalline SM55 at different irradiance (single diode model).

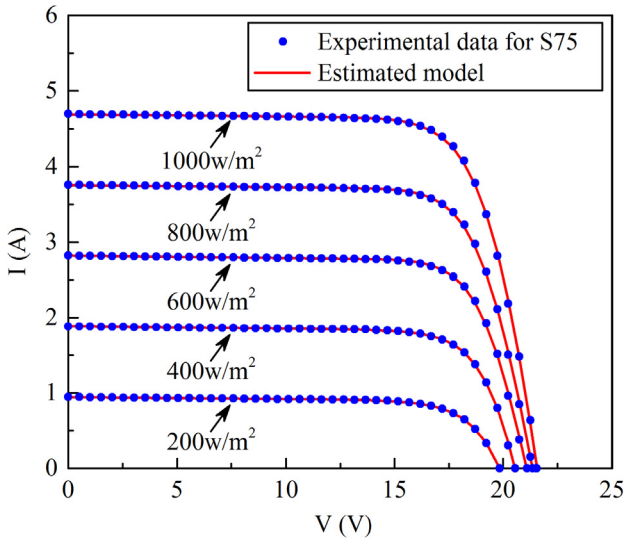


Fig. 17. Comparison between the estimated model and the experimental data of Multi-crystalline S75 at different irradiance (single diode model).

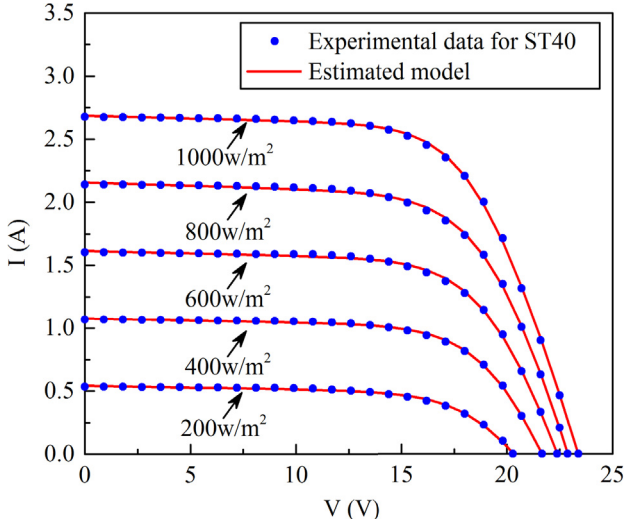


Fig. 18. Comparison between the estimated model and the experimental data of Thin-film ST40 at different irradiance (single diode model).

4.2.2. Case study 2: double diode model

The optimal parameters of the double diode model extracted for the three solar modules at different temperature values are given in Tables 12–14. Meanwhile, the optimal parameters extracted for them at different irradiance levels are given in Table 15. The comparisons between the estimated models and the experimental data of the three PV modules at different temperature values are given in Figs. 20–22 and at different irradiance levels are given in Figs. 23–25.

It can also be observed that, for all the three PV modules, the I-V curves of the estimated double diode models also strongly agree to the experimental data at all irradiance levels and temperature val-

Table 12

The extracted parameters for Multi-crystalline S75 PV module by GOFPANM at different temperature and irradiance of 1000 W/m^2 (double diode model).

Parameters	Temperature		
	(25 °C)	(50 °C)	(60 °C)
Multi-crystalline S75			
I_{ph} (A)	4.69670096	4.73280188	4.75588645
I_{sd1} (μA)	0.10129805	1.00000000	1.00000000
I_{sd2} (μA)	0.02420648	1.00000000	1.00000000
R_s (Ω)	0.25968045	0.26954362	0.31506631
R_{sh} (Ω)	373.62178865	2553.95254292	931.74873871
n_1	3.56812487	1.34530340	1.25830504
n_2	1.22198008	1.34530744	1.25831560
RMSE	0.02532194	0.02608539	0.03458788

Table 13

The extracted parameters for Thin-film ST40 PV module by GOFPANM at different temperature and irradiance of 1000 W/m^2 (double diode model).

Parameters	Temperature		
	(25 °C)	(40 °C)	(50 °C)
Thin-film ST40			
I_{ph} (A)	2.70362850	2.73743928	2.75946195
I_{sd1} (μA)	0.13906852	0.99999102	0.99999975
I_{sd2} (μA)	0.00115740	0.99999851	1.00000000
R_s (Ω)	1.31878820	1.15412152	1.25336113
R_{sh} (Ω)	217.16290827	168.26216154	136.60822953
n_1	1.33602188	1.36710360	1.26657588
n_2	1.04967757	1.36688813	1.26654781
RMSE	0.01873942	0.01551996	0.01796410

Table 14

The extracted parameters for Mono-crystalline SM55 PV module by GOFPANM at different temperature and irradiance of 1000 W/m² (double diode model).

Parameters	Temperature		
	(25 °C)	(40 °C)	(60 °C)
Mono-crystalline SM55			
I_{ph} (A)	3.41218666	3.41422769	3.44031603
I_{sd1} (μ A)	0.00023856	0.59327578	0.99998780
I_{sd2} (μ A)	0.00005101	0.00168372	0.02113895
R_s (Ω)	0.50877868	0.50063124	0.48178741
R_{sh} (Ω)	317.65533493	779.40436564	1347.22400695
n_1	1.00507642	1.54275300	1.29811957
n_2	1.35637256	1.00000000	1.00944026
RMSE	0.01225753	0.01006959	0.00969772

Table 15

The extracted parameters for three different types of PV modules by GOFPANM at different radiation and 25 °C (double diode model).

Parameters	Multi-crystalline S75	Thin-film ST40	Mono-crystalline SM55
$G = 1000 \text{ W/m}^2$			
I_{ph} (A)	4.69670096	2.70362850	3.41218666
I_{sd1} (μ A)	0.10129805	0.13906852	0.00023856
I_{sd2} (μ A)	0.02420648	0.00115740	0.00005101
R_s (Ω)	0.25968045	1.31878820	0.50877868
R_{sh} (Ω)	373.62178865	217.16290827	317.65533493
n_1	3.56812487	1.33602188	1.00507642
n_2	1.22198008	1.04967757	1.35637256
RMSE	0.02532194	0.01873942	0.01225753
$G = 800 \text{ W/m}^2$			
I_{ph} (A)	3.75642104	2.16336086	2.72793579
I_{sd1} (μ A)	0.61560883	0.99999977	0.00015771
I_{sd2} (μ A)	0.00327397	0.99999892	0.00122064
R_s (Ω)	0.35178096	1.04734110	0.53095436
R_{sh} (Ω)	425.94349003	220.67174418	393.95464173
n_1	3.93972467	1.53167403	1.00731968
n_2	1.10667510	1.53174051	1.13266801
RMSE	0.02231461	0.01325838	0.02496406
$G = 600 \text{ W/m}^2$			
I_{ph} (A)	2.82982773	1.61899217	2.04701888
I_{sd1} (μ A)	0.00007229	1.00000000	0.00016930
I_{sd2} (μ A)	0.00060509	0.99999997	0.12528252
R_s (Ω)	0.39319308	1.13603035	0.48945821
R_{sh} (Ω)	298.04906556	303.59474690	503.42779245
n_1	1.00028068	1.52940119	1.00089068
n_2	1.03475509	1.52937800	1.48806304
RMSE	0.02331863	0.01109699	0.01117934
$G = 400 \text{ W/m}^2$			
I_{ph} (A)	1.88422180	1.08112367	1.35816341
I_{sd1} (μ A)	0.60472491	0.99964766	0.95713713
I_{sd2} (μ A)	0.00635887	0.99933751	0.00871788
R_s (Ω)	0.26434392	1.21380182	0.32747230
R_{sh} (Ω)	350.08346862	346.57129354	1184.53465986
n_1	4.00000000	1.52590963	1.78073551
n_2	1.14058703	1.52914753	1.20033151
RMSE	0.00933519	0.00692279	0.00597013
$G = 200 \text{ W/m}^2$			
I_{ph} (A)	0.94411217	0.544465161	0.69460069
I_{sd1} (μ A)	0.13036208	1.00000000	0.00122920
I_{sd2} (μ A)	0.02518731	1.00000000	0.00139072
R_s (Ω)	0.26352152	1.82472097	0.70767132
R_{sh} (Ω)	411.69355972	377.09409259	282.75426933
n_1	2.70812551	1.51665004	1.34850072
n_2	1.23411188	1.51664990	1.07838692
RMSE	0.00159484	0.00691884	0.00250071

ues under investigation. The estimated models are also very accurate at low irradiance level.

From Tables 12–15, it can be found that, the values of the series resistance R_s falls within the interval [1,2] for Thin-film ST40, and is around 0.3 for Multi-crystalline S75 and around 0.5 for Mono-

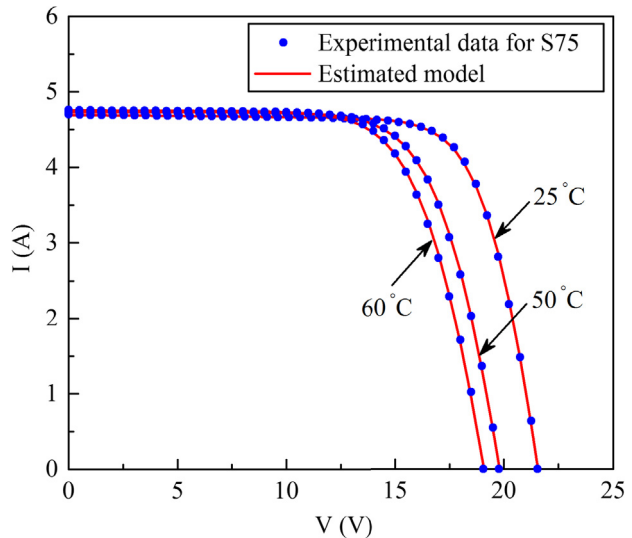


Fig. 20. Comparison between the estimated model and the experimental data of Multi-crystalline S75 at different temperature (double diode model).

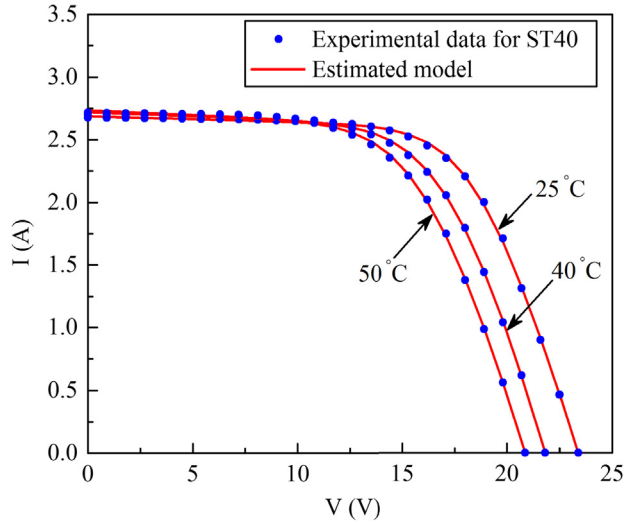


Fig. 21. Comparison between the estimated model and the experimental data of Thin-film ST40 at different temperature (double diode model).

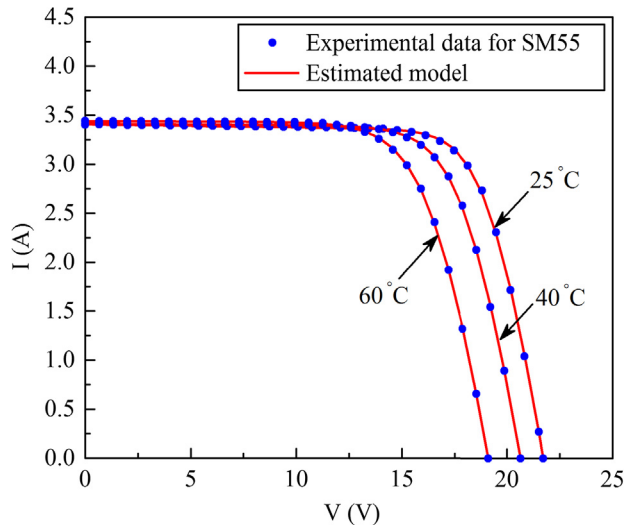


Fig. 22. Comparison between the estimated model and the experimental data of Mono-crystalline SM55 at different temperature (double diode model).

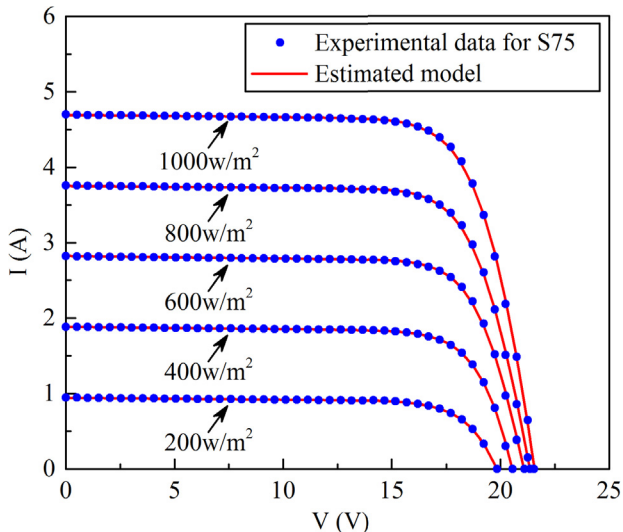


Fig. 23. Comparison between the estimated model and the experimental data of Multi-crystalline S75 at different irradiance (double diode model).

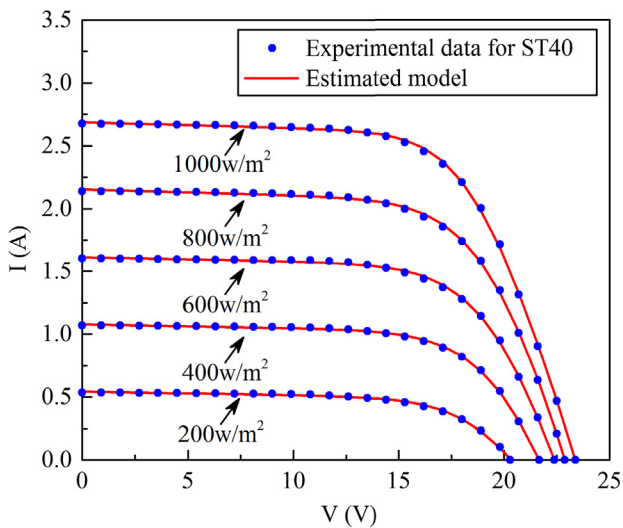


Fig. 24. Comparison between the estimated model and the experimental data of Thin-film ST40 at different irradiance (double diode model).

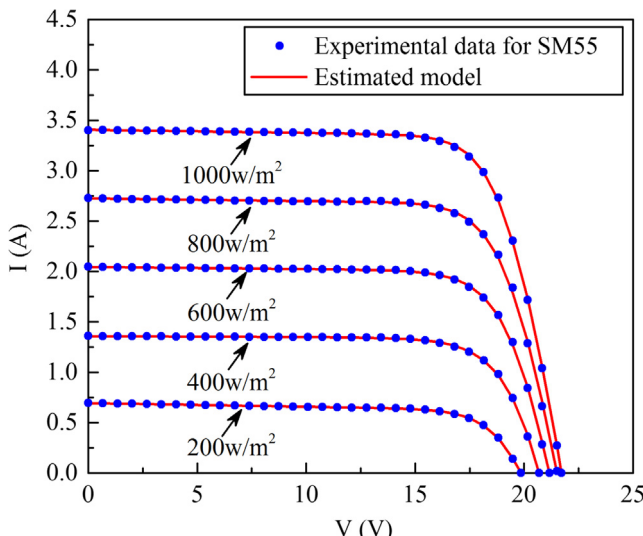


Fig. 25. Comparison between the estimated model and the experimental data of Mono-crystalline SM55 at different irradiance (double diode model).

crystalline SM55. Similarly with the results obtained previous, the series resistance R_s is very low and the parallel resistance R_{sh} is very high.

5. Conclusions

In this study, an improved variant of the flower pollination algorithm is proposed for estimating the parameters of solar cell models and PV modules quickly and accurately. The proposed algorithm integrates the basic flower pollination algorithm, the Nelder-Mead simplex method, and the generalized opposition-based learning mechanism together in a very simple way. Its performance is comprehensively examined on the parameter estimation problems of different solar cell models including the single diode model, the double diode model, and the PV module and compared with various published methods. Experimental and comparative results support that the proposed algorithm can extract the parameters accurately and efficiently and it is better or at least comparable to the other reported algorithms from literature. In addition, tests on three PV modules of different types at different irradiance levels and different temperature values further suggest that the proposed algorithm is effective and practical. Due to its potential shown in this study, the proposed algorithm can serve as a new alternative method for estimating the parameters of solar cells/PV modules.

The stability of the proposed algorithm should be further enhanced in future. As that showed in the double diode model case, there is still very little probability that the algorithm would trap into local optimal. Based on what have been observed during our experiments, this is mainly caused by the decline of the population diversity. Introducing population re-initialization mechanisms into the proposed algorithm may be a potential approach for alleviating this weakness.

Acknowledgements

The authors sincerely thank the anonymous reviewers for their constructive comments which greatly improved the quality of this paper and acknowledge the supports provided by the National Natural Science Foundation of China (Grant No. 51475270).

References

- [1] AlHajri MF, El-Naggar KM, AlRashidi MR, Al-Othman AK. Optimal extraction of solar cell parameters using pattern search. *Renew Energy* 2012;44:238–45.
- [2] AlRashidi MR, AlHajri MF, El-Naggar KM, Al-Othman AK. A new estimation approach for determining the I-V characteristics of solar cells. *Sol Energy* 2011;85:1543–50.
- [3] Baharoon DA, Rahman HA, Wan ZWO, Fadhl SO. Historical development of concentrating solar power technologies to generate clean electricity efficiently – a review. *Renew Sust Energy Rev* 2015;41:996–1027.
- [4] Parida B, Iniyar S, Goic R. A review of solar photovoltaic technologies. *Renew Sust Energy Rev* 2011;15:1625–36.
- [5] Nassar-eddine I, Obbadi A, Errami Y, El fajri A, Agunaou M. Parameter estimation of photovoltaic modules using iterative method and the Lambert W function: a comparative study. *Energy Convers Manage* 2016;119:37–48.
- [6] Kichou S, Abaslioglu E, Silvestre S, Nofuentes G, Torres-Ramirez M, Chouder A. Study of degradation and evaluation of model parameters of micromorph silicon photovoltaic modules under outdoor long term exposure in Jaén, Spain. *Energy Convers Manage* 2016;120:109–19.
- [7] Slimani MEA, Amirat M, Bahria S, Kurucz I, Aouli MH, Sellami R. Study and modeling of energy performance of a hybrid photovoltaic/thermal solar collector: configuration suitable for an indirect solar dryer. *Energy Convers Manage* 2016;125:209–21.
- [8] Slimani MEA, Amirat M, Kurucz I, Bahria S, Hamidat A, Chaouch WB. A detailed thermal-electrical model of three photovoltaic/thermal (PV/T) hybrid air collectors and photovoltaic (PV) module: comparative study under Algiers climatic conditions. *Energy Convers Manage* 2017;133:458–76.
- [9] Niu Q, Zhang H, Li K. An improved TLBO with elite strategy for parameters identification of PEM fuel cell and solar cell models. *Int J Hydrogen Energy* 2014;39:3837–54.
- [10] Bouraiou A, Hammouda M, Chaker A, Mostefaoui M, Lachtar S, Sadok M, et al. Analysis and evaluation of the impact of climatic conditions on the

- photovoltaic modules performance in the desert environment. *Energy Convers Manage* 2015;106:1345–55.
- [11] Niu Q, Zhang L, Li K. A biogeography-based optimization algorithm with mutation strategies for model parameter estimation of solar and fuel cells. *Energy Convers Manage* 2014;86:1173–85.
 - [12] Chen X, Yu K, Du W, Zhao W, Liu G. Parameters identification of solar cell models using generalized oppositional teaching learning based optimization. *Energy* 2016;99:170–80.
 - [13] Muhsen DH, Ghazali AB, Khatib T, Abed IA. Parameters extraction of double diode photovoltaic module's model based on hybrid evolutionary algorithm. *Energy Convers Manage* 2015;105:552–61.
 - [14] Chin VJ, Salam Z, Ishaque K. Cell modelling and model parameters estimation techniques for photovoltaic simulator application: a review. *Appl Energy* 2015;154:500–19.
 - [15] Askarzadeh A, Rezazadeh A. Artificial bee swarm optimization algorithm for parameters identification of solar cell models. *Appl Energy* 2013;102:943–9.
 - [16] Ismail MS, Moghavvemi M, Mahlia TMI. Characterization of PV panel and global optimization of its model parameters using genetic algorithm. *Energy Convers Manage* 2013;73:10–25.
 - [17] Zagrouba M, Sellami A, Bouaicha M, Ksouri M. Identification of PV solar cells and modules parameters using the genetic algorithms: application to maximum power extraction. *Sol Energy* 2010;84:860–6.
 - [18] Wei H, Cong J, Xue L, Song D. Extracting solar cell model parameters based on chaos particle swarm algorithm. In: International conference on electric information and control engineering (ICEICE). p. 398–402.
 - [19] Ye M, Wang X, Xu Y. Parameter extraction of solar cells using particle swarm optimization. *J Appl Phys* 2009;105:094502–94508.
 - [20] Khanna V, Das BK, Bisht D, Vandana, Singh PK. A three diode model for industrial solar cells and estimation of solar cell parameters using PSO algorithm. *Renew Energy* 2015;78:105–13.
 - [21] Ishaque K, Salam Z. An improved modeling method to determine the model parameters of photovoltaic (PV) modules using differential evolution (DE). *Sol Energy* 2011;85:2349–59.
 - [22] Jiang LL, Maskell DL, Patra JC. Parameter estimation of solar cells and modules using an improved adaptive differential evolution algorithm. *Appl Energy* 2013;112:185–93.
 - [23] Gong W, Cai Z. Parameter extraction of solar cell models using repaired adaptive differential evolution. *Sol Energy* 2013;94:209–20.
 - [24] Askarzadeh A, Rezazadeh A. Parameter identification for solar cell models using harmony search-based algorithms. *Sol Energy* 2012;86:3241–9.
 - [25] Jamadi M, Merrikh-Bayat F, Bigdeli M. Very accurate parameter estimation of single- and double-diode solar cell models using a modified artificial bee colony algorithm. *Int J Energy Environ Eng* 2016;7:13–25.
 - [26] Oliva D, Cuevas E, Pajares G. Parameter identification of solar cells using artificial bee colony optimization. *Energy* 2014;72:93–102.
 - [27] Hasanien HM. Shuffled frog leaping algorithm for photovoltaic model identification. *IEEE Trans Sust Energy* 2015;6:509–15.
 - [28] Allam D, Yousri DA, Eteiba MB. Parameters extraction of the three diode model for the multi-crystalline solar cell/module using Moth-Flame Optimization Algorithm. *Energy Convers Manage* 2016;123:535–48.
 - [29] Askarzadeh A, Coelho LDS. Determination of photovoltaic modules parameters at different operating conditions using a novel bird mating optimizer approach. *Energy Convers Manage* 2015;89:608–14.
 - [30] Askarzadeh A, Rezazadeh A. Extraction of maximum power point in solar cells using bird mating optimizer-based parameters identification approach. *Sol Energy* 2013;90:123–33.
 - [31] Yang X-S. Flower pollination algorithm for global optimization. In: Durand-Lose J, Jonoska N, editors. *Unconventional computation and natural computation*. Berlin, Heidelberg: Springer; 2012. p. 240–9.
 - [32] Yang X-S, Karamanoglu M, He X. Flower pollination algorithm: a novel approach for multiobjective optimization. *Eng Optimiz* 2013;46:1222–37.
 - [33] Dash P, Saikia LC, Sinha N. Flower pollination algorithm optimized PI-PD cascade controller in automatic generation control of a multi-area power system. *Int J Electr Power* 2016;82:19–28.
 - [34] Bekdas G, Nigdeli SM, Yang XS. Sizing optimization of truss structures using flower pollination algorithm. *Appl Soft Comput* 2015;37:322–31.
 - [35] Xu S, Wang Y, Huang F. Optimization of multi-pass turning parameters through an improved flower pollination algorithm. *Int J Adv Manuf Technol* 2017;89:503–14.
 - [36] Dubey HM, Pandit M, Panigrahi BK. Hybrid flower pollination algorithm with time-varying fuzzy selection mechanism for wind integrated multi-objective dynamic economic dispatch. *Renew Energy* 2015;83:188–202.
 - [37] Chiroma H, Khan A, Abubakar AI, Saadi Y, Hamza MF, Shuib L, et al. A new approach for forecasting OPEC petroleum consumption based on neural network train by using flower pollination algorithm. *Appl Soft Comput* 2016;48:50–8.
 - [38] Alam DF, Yousri DA, Eteiba MB. Flower Pollination Algorithm based solar PV parameter estimation. *Energy Convers Manage* 2015;101:410–22.
 - [39] Humada AM, Hojabri M, Mekhilef S, Hamada HM. Solar cell parameters extraction based on single and double-diode models: a review. *Renew Sust Energy Rev* 2016;56:494–509.
 - [40] Wolf M, Noel GT, Stirn RJ. Investigation of the double exponential in the current-Voltage characteristics of silicon solar cells. *IEEE Trans Electron Dev* 1977;24:419–28.
 - [41] Villalva MG, Gazoli JR, Filho ER. Comprehensive approach to modeling and simulation of photovoltaic arrays. *IEEE Trans Power Electr* 2009;24:1198–208.
 - [42] Nelder JA, Mead R. A simplex method for function minimization. *Comput J* 1965;7:308–13.
 - [43] Olsson DM, Nelson LS. The Nelder-Mead simplex procedure for function minimization. *Technometrics* 1975;17:45–51.
 - [44] Fan S-KS, Zahara E. A hybrid simplex search and particle swarm optimization for unconstrained optimization. *Eur J Oper Res* 2007;181:527–48.
 - [45] Maehara N, Shimoda Y. Application of the genetic algorithm and downhill simplex methods (Nelder-Mead methods) in the search for the optimum chiller configuration. *Appl Therm Eng* 2013;61:433–42.
 - [46] Zahara E, Kao Y-T. Hybrid Nelder-Mead simplex search and particle swarm optimization for constrained engineering design problems. *Expert Syst Appl* 2009;36:3880–6.
 - [47] Tizhoosh H. Opposition-based learning: a new scheme for machine intelligence. In: International conference on computational intelligence for modelling, control and automation and international conference on intelligent agents, Web Technologies and Internet Commerce (CIMCA-IAWTIC'06)2005. p. 695–701.
 - [48] Al-Qunaieer FS, Tizhoosh HR, Rahnamayan S. Opposition based computing—a survey. In: The 2010 international joint conference on neural networks (IJCNN). IEEE; 2010. p. 1–7.
 - [49] Sahba F, Tizhoosh HR, Salama MM. Application of opposition-based reinforcement learning in image segmentation. In: IEEE symposium on computational intelligence in image and signal processing. IEEE; 2007. p. 246–51.
 - [50] Tizhoosh HR. Opposite fuzzy sets with applications in image processing. In: IFSA/EUSFLAT conf Citeseer. p. 36–41.
 - [51] Tizhoosh HR, Sahba F. Quasi-global oppositional fuzzy thresholding. In: IEEE international conference on fuzzy systems. IEEE; 2009. p. 1346–51.
 - [52] Ventresca M, Tizhoosh HR. Opposite transfer functions and backpropagation through time. In: IEEE symposium on foundations of computational intelligence. IEEE; 2007. p. 570–7.
 - [53] Ventresca M, Tizhoosh HR. Simulated annealing with opposite neighbors. In: IEEE symposium on foundations of computational intelligence. IEEE; 2007. p. 186–92.
 - [54] Ventresca M, Tizhoosh HR. A diversity maintaining population-based incremental learning algorithm. *INFORM SCIENCES* 2008;178:4038–56.
 - [55] Ahmandani M, Alavi-Rad H. Opposition-based learning in the shuffled differential evolution algorithm. *Soft Comput* 2012;16:1303–37.
 - [56] Wang H, Wu Z, Liu Y, Wang J, Jiang D, Chen L. Space transformation search: a new evolutionary technique. In: Proceedings of the first ACM/SIGEVO summit on genetic and evolutionary computation. ACM; 2009. p. 537–44.
 - [57] Wang H, Rahnamayan S, Wu Z. Parallel differential evolution with self-adapting control parameters and generalized opposition-based learning for solving high-dimensional optimization problems. *J Parallel Distrib Comput* 2013;73:62–73.
 - [58] Wang H, Wu Z, Rahnamayan S. Enhanced opposition-based differential evolution for solving high-dimensional continuous optimization problems. *Soft Comput* 2011;15:2127–40.
 - [59] Wang H, Wu Z, Rahnamayan S, Liu Y, Ventresca M. Enhancing particle swarm optimization using generalized opposition-based learning. *Inform Sci* 2011;181:4699–714.
 - [60] Easwarakhanthan T, Bottin J, Bouhouc I, Boutrit C. Nonlinear minimization algorithm for determining the solar cell parameters with microcomputers. *Int J Solar Energy* 1986;4:1–12.
 - [61] Dkhichi F, Oukarfi B, Fakkari A, Belbounaguia N. Parameter identification of solar cell model using Levenberg–Marquardt algorithm combined with simulated annealing. *Sol Energy* 2014;110:781–8.
 - [62] El-Naggar KM, AlRashidi MR, AlHajri MF, Al-Othman AK. Simulated Annealing algorithm for photovoltaic parameters identification. *Sol Energy* 2012;86:266–74.
 - [63] Bouzidi K, Chegaar M, Nehaoua N. New method to extract the parameters of solar cells from their illuminated IV curve. In: 4th international conference on computer integrated manufacturing, Setif, Algeria; 2007. p. 1–4.
 - [64] Chegaar M, Nehaoua N, Bouhemadou A. Organic and inorganic solar cells parameters evaluation from single I-V plot. *Energy Convers Manage* 2008;49:1376–9.
 - [65] Shell S75 Photovoltaic Solar Module. <http://www.aeet-service.com/pdf/shell/Shell-Solar_S75.pdf>.
 - [66] Shell ST40 Photovoltaic Solar Module. <http://www.aeet-service.com/pdf/shell/Shell-Solar_ST40.pdf>.
 - [67] Shell SM55 Photovoltaic Solar Module. <http://www.aeet-service.com/pdf/shell/Shell-Solar_SM55.pdf>.